Reprinted from ENVIRONMENTAL SCIENCE & TECHNOLOGY, Vol. 26, 1992

Transport of Inorganic Colloids through Natural Aquifer Material: Implications for Contaminant Transport

Robert W. Puls*,† and Robert M. Powell‡

Robert S. Kerr Environmental Research Laboratory, U.S. EPA, P.O. Box 1198, Ada, Oklahoma 74820, and ManTech Environmental Technology, Inc., Robert S. Kerr Environmental Research Laboratory, P.O. Box 1198, Ada, Oklahoma 74820

■ The stability and transport of radiolabeled Fe_2O_3 particles were studied using laboratory batch and column techniques. Core material collected from a shallow sand and gravel aquifer was used as the immobile column matrix material. Variables in the study included flow rate, pH, ionic strength, electrolyte composition, particle concentration, and particle size. Transport was highly dependent upon colloidal stability. Iron oxide colloids were not only mobile to a significant extent, but under some hydrogeochemical conditions were transported faster than tritiated water, a conservative tracer. The extent of colloid breakthrough was dependent upon a variety of parameters; however, the highest statistical correlation was observed with particle size and anionic composition of the supporting electrolyte. Arsenate was utilized for assessment of colloid–contaminant and contaminant–aquifer interactions and comparison of dissolved and colloidally associated transport in dynamic model systems. The rate of colloid-associated arsenate transport was over 21 times that of the dissolved arsenate.

Introduction

Models which predict the transport of inorganic contaminants in subsurface systems have traditionally been based on a two-phase approach: the mobile fluid phase and the immobile solid phase. A gradual consensus has developed over the past several years, however, that a three-phase approach, one which incorporates a mobile solid phase, may be necessary under some hydrogeochemical conditions. These are solid particles of colloidal dimensions. Colloids are generally regarded as particles having diameters less than 10 μm (*1*), which tend to remain suspended in water. Several researchers have investigated the mobility of colloidal particles in subsurface systems. Gschwend and Reynolds (*2*) demonstrated that submicron ferrous phosphate colloids were suspended and presumably mobile in a sand and gravel aquifer. Robertson (*3*) found that tannin and lignin from a waste pulp liquor plume migrated in a sand aquifer at close to the average linear groundwater flow velocity. Ryan and Gschwend (*4*) found that, under anoxic conditions, soil colloids were mobilized due to dissolution of ferric oxyhydroxide coatings that cemented clay particles to aquifer solids. Wellings (*5*) and Mack (*6*) demonstrated the long-distance transport of colloidal viruses through soils into groundwater. Field studies by Nightingale and Bianchi (*7*) showed that, under certain conditions, submicron-sized particles within the surface-weathered zone are mobilized for some distance both vertically and laterally and affect groundwater turbidity.

Due to their high specific surface area and reactivity, mobile inorganic particles consisting of clay minerals, hydrous iron, and aluminum oxides may significantly affect the transport of contaminants. In a study by Kim et al. (*8*), it was suggested that the transport of some radionuclides in groundwater at Gorleben, Germany, was facilitated by the presence of mobile ferric hydroxide particles. Torok et al. (*9*) found that Cs transport through soils was primarily controlled by sorption onto clay particles followed by clay particle transport. Others have demonstrated the facilitated transport of contaminants associated with reactive mobile colloidal particles in both laboratory and field studies (*10–14*). In addition to high reactivity, colloids must be present in relatively high concentrations to be a significant transport mechanism. Recent estimates of colloidal concentrations in groundwater range as high as 63 mg/L (*4*, *14*, *15*).

Particles with diameters of 0.1–2.0 μm may constitute the most mobile size fraction in porous media. The efficiency of particle removal increases rapidly beyond 1 μm due to sedimentation and/or interception processes, whereas for particles smaller than 0.1 μm, removal occurs by diffusion (*16*, *17*). In laboratory experiments using sand columns and carboxylated polystyrene beads that ranged in size from 0.10 to 0.91 μm as model colloids, Reynolds (*18*) recovered 45% of the 0.91-μm and greater than 70% of 0.10- and 0.28-μm beads. Data of Rundberg in a report by Nuttall (*19*) have shown greater breakthrough of 0.91- than 0.1-μm particles in fracture flow column experiments for the Yucca Mountain project. Penrose et al. (*12*) found detectable amounts of plutonium and americium, 3390-m downgradient from a source, to be tightly or irreversibly associated with particles between 0.025 and 0.45 μm in size.

While considerable evidence has been gathered to support the occurrence and environmental significance of colloid mobility, there has been very little work investigating the specific geochemical controls on colloid stability and transport in natural systems. Cerda (*20*) demonstrated that the mobilization of kaolinite fines in laboratory columns was almost totally dependent upon the chemistry of the fluids present, with maximum mobility occurring under relatively high saline, weakly alkaline pH conditions. Repulsive colloidal forces promoting stability were in evidence up to 0.1 M NaCl (pH 9). In laboratory tests, Eichholz et al. (*21*) found that cationic nuclides were competitively adsorbed on suspended clay particles that were shown to be capable of traveling at water flow velocity in porous mineral columns. In simulated aquifer experiments using sand beds, Champlin and Eichholz (*22*) demonstrated that previously "fixed" particles and associated contaminants may be remobilized by changes in the aqueous geochemistry of the system. Matijevic et al. (*23*) studied the stability and transport of hematite spheres through packed-bed columns of stainless-steel beads as a function of pH and the concentration of a variety of simple and complex electrolytes. Surface charge alterations of the hematite and stainless-steel beads by different electrolytes was the dominant factor in particle deposition and detachment.

Most research efforts have utilized artificial laboratory model systems (e.g., fluorescent latex microspheres, glass beads, stainless-steel beads, etc.). The purpose of this work was to investigate specific aqueous chemical effects on the mobility of environmentally realistic colloids and their

† U.S. EPA.
‡ ManTech Environmental Technology, Inc.

0013-936X/92/0926-0614$03.00/0

Table I. X-Ray Diffraction Data for Aquifer Solids from Well 107, Globe, AZ

intensity,* %	mineral phase	chemical formula
100	quartz	SiO_2
52	albite	$NaAlSi_3O_8$
17	magnesium orthoferrosilite	$(Fe,Mg)SiO_3$
17	grunlingite	Bi_4TeS_3
15	taeniolite	$K_{1.3}Mg_{4.6}Li_{1.25}Si_{7.98}O_{20.05}F_{3.97}$
12	muscovite	$KAl_2(Si_3Al)O_{10}(OH,F)_2$
12	raguinite	$TiFeS_2$
10	hercynite	$FeAl_2O_4$
5	manganese dioxide	MnO_2

* Intensity is relative abundance with the predominant peak arbitrarily set at 100% and the remaining peaks normalized to that peak height.

potential for transport through natural porous aquifer media under controlled laboratory conditions. Iron oxide particles were synthesized to specific size and shape for use as the mobile colloidal phase. These were deemed more realistic in terms of their surface charge and density characteristics. Aquifer material collected from a research site in Globe, AZ, was used for the column packing material or immobile phase. Arsenate was selected as a ubiquitous and hazardous inorganic contaminant. Batch experiments were performed to evaluate colloid stability and assess the interactions between the iron oxide particles, the aquifer matrix, and the dissolved arsenate. Column experiments were performed to determine the extent of colloid transport and to compare retardation of aqueous and colloid-associated arsenate. Study variables included column flow rate, pH, ionic strength, electrolyte composition (anion/cation), particle concentration, and particle size.

Materials and Methods

All solutions and suspensions were prepared from deionized water (DIW, Millipore Corp.). Glassware was cleaned in 10% HNO_3 and rinsed several times with DIW before use. Reagents were analytical grade (Fisher Scientific and Aldrich Chemical) and used as received.

Aquifer Solids. Core material was collected from a site at Pinal Creek, near Globe, AZ. Previous research at this site has focused on colloidal considerations in sampling groundwaters for inorganic contaminants (*24*). Copper has been mined since 1903 from granite porphyry adjacent to an aquifer at the site. A band of unconsolidated alluvium 300–800 m wide, as much as 50 m thick, and ~20 km long forms the upper, central part of the aquifer in a valley along Miami Wash and Pinal Creek. Most of the sediment in the alluvium ranges in size from fine sand to coarse gravel, but clay lenses and boulders are also present. Alluvial, consolidated, basin fill, more than 100 m thick, forms the remainder of the aquifer beneath and adjacent to the unconsolidated alluvium.

In the upper alluvium, hydraulic conductivity is on the order of 200 m/day on the basis of cross-sectional area, hydraulic gradient, and measured outflow (*25*). On the basis of hydraulic gradients that range from 0.005 to 0.008, the Darcy velocities near the wells in the upper alluvium range from 1.0 to 1.7 m/day.

The major mineral phases in the aquifer samples were identified with X-ray diffraction (XRD) and are listed in Table I. The pH_{pzc}, or pH at which the net surface charge of a solid equals zero, is an important parameter affecting both colloidal stability and the interaction of the colloids with immobile matrix surfaces. Above the pH_{pzc}, minerals possess a net negative charge, while below this pH, the net charge is positive. Due to the predominance of silica (pH_{pzc} ~ 2) and other minerals such as layer silicates and manganese oxides, which have pH_{pzc}'s < 4, it was assumed that the column matrix material would exhibit a net negative charge under most environmentally relevant pH conditions.

Figure 1. Scanning electron micrograph of approximately 200 nm diameter Fe_2O_3 particles.

Synthesis of Fe_2O_3 Colloids. Spherical, monodisperse Fe_2O_3 colloids (100–300 nm) were prepared from solutions of $FeCl_3$ and HCl using the method of Matijevic and Scheiner (*26*). The method was modified by the addition of a spike of $^{59}FeCl_3$, prior to heating, to permit detection of the colloid with liquid scintillation counting techniques. The colloids were washed repeatedly with pH 3 deionized water to remove unreacted materials from the suspensions. Particle concentration was determined by both filtration and residue on evaporation techniques to be ~1.5 g/L. Mass balances were performed to verify the results. Scanning electron microscopy (SEM) and photon correlation spectroscopy (PCS) were used to confirm particle size and shape. Figure 1 is a scanning electron micrograph of the ~200-nm synthesized spherical iron oxide particles. The surface area of 200-nm uniformly spherical particles was calculated to be 5.72 m^2/g using the equation

$$A = 6 \times 10^{-4}/\rho d \qquad (1)$$

where A is the geometric surface area, ρ the density, and d the diameter. While this probably underestimates the actual surface area due to surface roughness, microporosity, and shape, it does provide a reasonable estimate.

Fe_2O_3 Surface Characterization. Acid–base titrations and particle microelectrophoresis were used to characterize the surface charge properties of the synthesized particles. Acid–base titrations of the Fe_2O_3 particles were performed manually in a glovebox under nitrogen, and on the benchtop using an Orion 960 autotitrator. Measurements were taken using an Orion Ross electrode and additions of acid or base were recorded carefully. Solutions 0.01 M in NaOH, HCl, or $HClO_4$ were standardized against potassium hydrogen phthalate and used as the titrants.

The titrations performed on the benchtop with the autotitrator were purged by high-purity N_2 gas, which had been additionally stripped of CO_2 with an in-line Ascarite filter. Aliquots (30 mL) of washed colloids were placed in 180-mL tall-form beakers. Ionic strength adjustments were made using appropriate weights of $NaClO_4$ crystals dissolved into the suspension. The suspensions were adjusted to a starting pH of 4 and allowed to equilibrate for at least 24 h. Titrant additions were programmed for 10-min intervals.

The glovebox titrations were performed by manually adding the titrant to 30-mL colloidal suspensions using a microliter pipet. Ionic strength adjustments were made using appropriate weights of NaCl crystals dissolved into the suspension, which was then allowed to equilibrate overnight in the glovebox. Titrant additions were made when the pH of the suspension appeared stable within the measuring limits of the electrode (±0.02–0.04 pH/min). This interval ranged from a low of 13 min away from the pH_{zpc} to 25 min in its vicinity.

Electrophoretic mobility (EM) of the colloids was determined using a Rank Brothers Mark II system with a four-electrode capillary cell, thermostated at 30 °C, that was illuminated by a 3-mW neon–helium laser. The system was fitted with a video camera coupled to a rotating prism for acquiring mobility data. Fe_2O_3 suspensions were prepared at 1:100 dilutions of the washed stock colloidal suspensions, in various electrolytes, to cover a pH range from approximately 3 to 10. $NaClO_4$ at two ionic strengths, 0.001 and 0.01 M, was utilized as a relatively noninteractive electrolyte to determine the pH of zero mobility or isoelectric point (pH_{iep}) of the colloids in the absence of specifically sorbed species. Mobility was then determined in 0.01 M NaH_2PO_4 and 0.01 M Na_2HAsO_4, both specifically sorbed anions, to assess their impact on electrophoretic mobility over a range of pH. The constant voltage applied to the cell was 25 V, 19.5 V as measured across the probe electrodes.

Arsenate Adsorption Experiments. Adsorption of arsenate to the aquifer solids was performed to determine its affinity for these surfaces and for comparison of batch and column-derived solid–solution distribution values. Adsorption of arsenate to the Fe_2O_3 particles was also investigated to determine the adsorption capacity of the particles and strength of arsenate retention. Preliminary experiments were performed to determine steady-state equilibration time and appropriate solid–solution ratio. A 24-h equilibration period and solid–solution ratios of 6 g/30 mL for the aquifer solids and 4.5 mg/30 mL for the Fe_2O_3 particles were chosen. Triplicate sorption–desorption experiments were performed in 50-mL Oak Ridge polyallomer centrifuge tubes. Initial arsenate concentrations ranged from 7×10^{-6} to 3×10^{-4} M in 0.01 M $NaClO_4$. The pH range examined was 4–8, and a temperature of approximately 25 °C was used in all experiments. Samples were shaken on a rotary shaker throughout the equilibration to ensure mixing. After equilibration, samples were centrifuged at 2560*g* for 70 min. The supernatant was additionally filtered through 0.2-μM Nuclepore membrane filters to prevent the inclusion of solid flocs and microparticles in determinations of aqueous concentrations of arsenate. Samples were acidified with double-distilled HNO_3 to pH <2 for analysis with a Jarrell-Ash Model 975 inductively coupled argon plasma (ICAP) or a Perkin-Elmer Zeeman/3030 atomic absorption spectrophotometer with graphite furnace (AAGF). Adsorption was determined by difference between initial and final arsenate concentrations. Desorption of arsenate from both the iron oxide particles and the aquifer solids was accomplished by repeated replacement of the centrate with arsenate-free 0.01 M $NaClO_4$ following adsorption. In all experiments, blanks and stock standards were analyzed and losses to containers and filters were evaluated.

Colloid/Matrix Interaction Experiments. Interaction of the Fe_2O_3 particles with the aquifer solids was evaluated in batch experiments for comparison with column results. The duration of these experiments was 1 h with shaking, comparable to the colloid–matrix contact time for the slowest flow rate used in the column tests. The same solid/solution ratios were used as for the adsorption experiments, with triplicate samples and similar use of blanks. Separation of the radiolabeled particles from the aquifer solids was accomplished by allowing the samples to settle for 1 h, followed by withdrawal of 5 mL of supernatant, which was filtered through a 5-μm Nuclepore filter. Efficiency of 100-nm Fe_2O_3 particle passage through the 5-μm filters was determined to be >99% using the stock colloidal suspension.

Colloid Stability Experiments. Colloid stability was evaluated using PCS. Washed stock colloidal suspensions were used to spike solutions of various electrolyte composition, ionic strength, and pH. Samples were allowed to equilibrate overnight and the pH was readjusted as necessary. An increase in size of the Fe_2O_3 particles indicated instability. In the pH range where the particles were most unstable, coagulation was almost instantaneous. Selected samples were periodically rechecked over several weeks for confirmation of long-term stability.

Column Transport Experiments. Adjustable-length glass columns, 2.5-cm diameter, were used for all experiments. An Ismatec variable-speed peristaltic pump and an Isco Cygnet fraction collector were also used. Aquifer solids were air-dried and sieved, with the 106–2000-μm fraction used to pack the columns to bulk densities ranging from 1.5 to 1.7 g/cm^3. Assuming a particle density of 2.65 g/cm^3 for the aquifer solids, the porosity ranged from 0.36 to 0.45. Porous polyethylene beds and 80-μm nylon screens were used to support the matrix aquifer solids in the column and allowed greater than 99% passage of colloids through the apparatus during blank runs. Columns were slowly (0.08 m/day) saturated from below and flushed for at least 1 week prior to initiation of experimental runs. Darcy velocities used in the experiments were 0.8, 1.7, and 3.4 m/day. Seven different columns were packed for numerous distinct experiments. The use of multiple columns was necessary as the injected particles became increasingly concentrated near the column inlet zone. The number of different experiments performed on any given column was therefore dependent upon previous experimental results. Columns were carefully examined when dismantled to assess the distribution of retained particles. The first two columns were operated in a vertical mode with suspensions injected from the top. The third column was operated both vertically and horizontally. Replicate runs indicated no significant differences with column orientation. The remaining four columns were operated horizontally. Tritiated water (^3HHO) was used as a conservative tracer to analyze column operation, as well as for transport comparisons with the injected particles and dissolved arsenate. Tritiated water and arsenate were injected until effluent concentration equaled influent concentration (C_o). For the colloidal transport experiments, the colloidal suspension and tritiated water injection durations were equal. The input of the Fe_2O_3 suspensions and arsenate was followed by background electrolyte of the same composition used for the injectates. PCS was used to verify size and stability of column influent colloidal suspensions, and comparisons were also made with selected column effluent samples. The effluent fractions were collected in polypropylene test tubes over various time intervals depending upon the flow rate and experiment (longer collection times for the dissolved arsenate experiments). A 0.5-mL aliquot from each fraction was mixed with Beckman CP cocktail in 7-mL polyethylene vials and counted on a (Beckman model) scintillation spectrophotometer for 20 min for the radiolabeled colloid experiments. The ar-

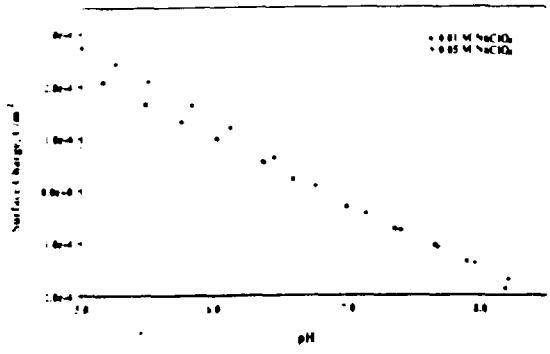

Figure 2. Surface charge on Fe_2O_3 particles as a function of pH in the presence of different concentrations of $NaClO_4$.

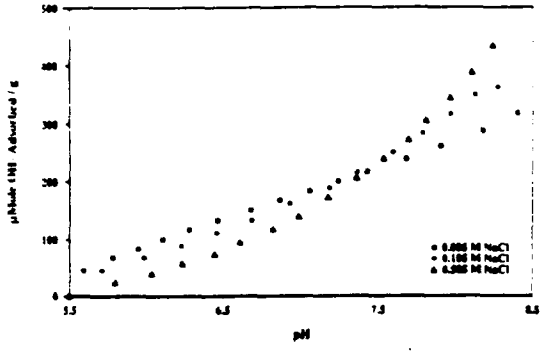

Figure 3. Potentiometric titrations of Fe_2O_3 particles as a function of pH in the presence of different concentrations of NaCl.

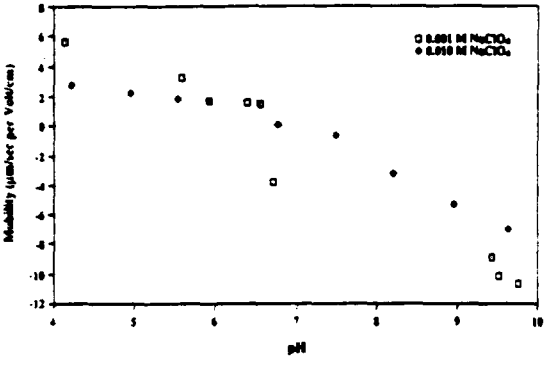

Figure 4. Electrophoretic mobility of Fe_2O_3 particles as a function of pH in the presence of different concentrations of $NaClO_4$.

senate experiments were analyzed by ICAP and AAGF.

Results and Discussion

Fe_2O_3 Surface Characterization. Results for the bench autotitrations ($NaClO_4$ background) and the manual glovebox titrations (NaCl background) are presented in Figures 2 and 3, respectively. The titration curves in Figure 2 converge at approximately pH 7; however, the curves never fully separate again. This is probably due to insufficient equilibration times between titrant additions in this region. Figure 3 provides a much more distinct crossover, indicating that sufficient equilibration time was allowed for these titrations, but it occurs at a higher pH, approximately pH 7.3–7.6.

Figures 4 and 5 illustrate the results of electrophoretic mobility determinations in the absence and presence of

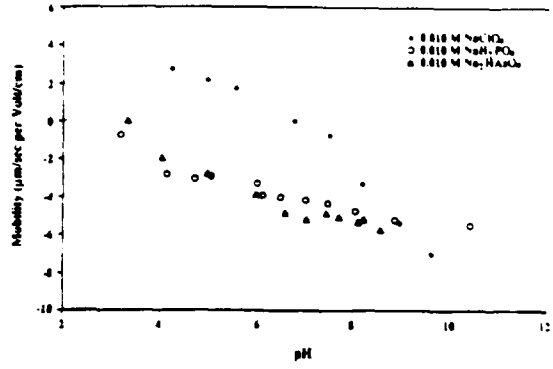

Figure 5. Electrophoretic mobility of Fe_2O_3 particles as a function of pH in the presence of 0.01 M sodium electrolytes of different anionic composition.

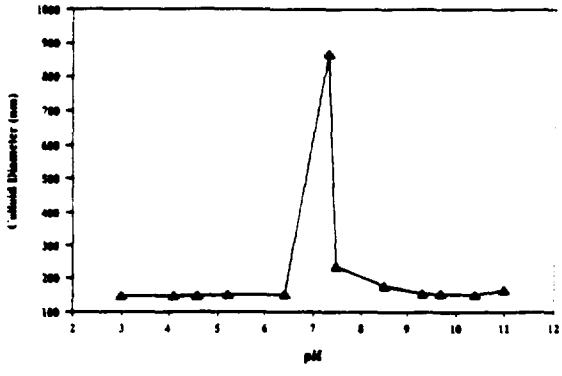

Figure 6. Stability of 150-nm Fe_2O_3 particles as a function of pH in 0.005 M $NaClO_4$.

strongly interacting anions, respectively. The pH_{zpc} is approximately 6.8 in the $NaClO_4$, which corresponds to the autotitration results in $NaClO_4$ (Figure 2). Matijevic et al. (*23*) found the pH_{zpc} for similarly synthesized particles to be pH ~7.

Relatively high concentrations of phosphate have been observed to enhance colloidal stability through charge reversal on positively charged particles (*27*), resulting in surfaces exhibiting an effective net negative charge at pH $\ll pH_{zpc}$. This was tested and observed for both phosphate and arsenate (Figure 5). This charge-reversal effect could have significant implications in the subsurface if sufficient amounts of specifically sorbing anions are present and capable of increasing the repulsion between individual colloidal particles (increased stability) as well as between the mobile particles and the immobile matrix minerals, thus promoting their transport.

Fe_2O_3 Colloid Stability. The stability of 150-nm Fe_2O_3 particles, suspended in 0.005 M $NaClO_4$, from pH 3 to 11, is shown in Figure 6. The Fe_2O_3 particles were stable in 0.01 M $NaClO_4$ and 0.01 M NaCl over the pH ranges 2.0–6.5 and 9.7–11.0. From pH 6.5 to 7.6, in the vicinity of the pH_{zpc}, the colloids were very unstable, even in extremely dilute electrolytes or deionized water. In 0.005 M $NaClO_4$ and 0.005 M NaCl, from pH 7.6 to 9.7, the colloids were quasi-stable; that is, the kinetics of coagulation were slow (several hours). This was also observed in 0.01 M Na_2SO_4 over the pH range 7.6–11. Therefore, column influent and effluent particle size was monitored throughout the column experiments.

An example of increasing particle size with the onset of coagulation or instability is shown in Figure 7. Over the

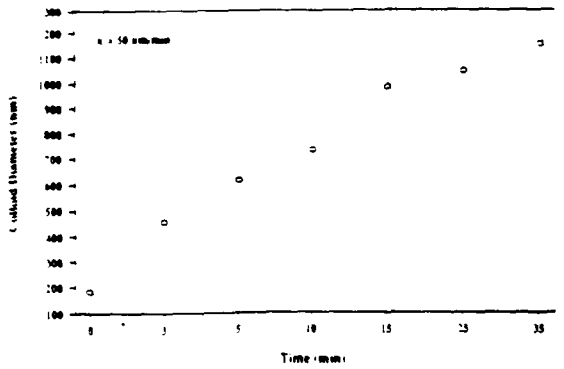

Figure 7. Coagulation kinetics of 150-nm Fe_2O_3 particles in 0.005 M $NaClO_4$ at pH 7.1.

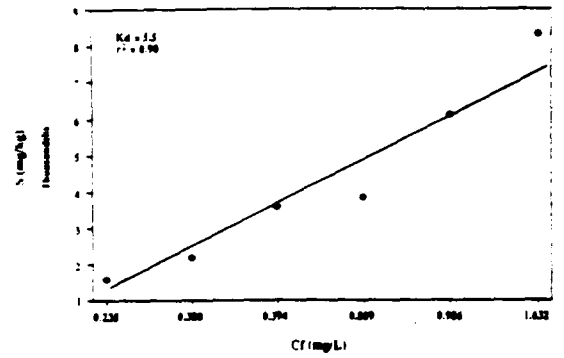

Figure 8. Freundlich isotherm data for arsenate adsorption on Globe, Az, aquifer solids (pH 7, 0.01 M $NaClO_4$, 6 g/30 mL, 24-h equilibration).

time and size range observed, the kinetics approximated a zero-order reaction rate. Up to ~1 μm, that apparent rate was 50 nm/min (r^2 = 0.94) as determined by PCS. This represents only a loose approximation due to uncertainties concerning particle packing.

When suspended in sodium arsenate or sodium phosphate solutions up to 0.01 M, the particles were stable from pH 4 to 11, as indicated above. In addition to increasing the pH stability region where the particles are net negatively charged, the magnitude of that charge is increased at a given pH by these multivalent anions, thus contributing to enhanced stability of the iron oxide particles over the pH range of these experiments.

Adsorption Experiments. Arsenate adsorption on the aquifer solids conformed to a Freundlich isotherm (Figure 8), defined by the relation

$$S = KC_f^n \tag{2}$$

where K is the empirical distribution coefficient or solid surface affinity term, S the steady-state concentration on the solids (mg/kg), C_f the steady-state solution concentration (mg/L), and n an empirical coefficient related to the monolayer capacity and energy of adsorption. Values of $n < 1$ imply decreasing energy of sorption with increasing surface coverage. The calculated K and n values, using the linearized form of the above equation, were 5.5 and 0.73, respectively.

Arsenate adsorption data for the Fe_2O_3 colloids were fitted to a Langmuir isotherm (Figure 9) defined by the relation

$$S = kbC_f/(1 + kC_f) \tag{3}$$

where k is the Langmuir solid surface distribution coefficient, b is the adsorption capacity, and S and C_f are defined above. An advantage of the Langmuir model is the incorporation of the capacity term. This is important for estimating the mass of contaminant potentially transported by the iron oxide particles. The correlation coefficient for the linearized Langmuir form of the above equation was 0.97 and the adsorption capacity was estimated to be 0.01 g of arsenic/g of Fe_2O_3. There was very little difference in adsorption from pH 4 to 7; however, a gradual decrease was observed with increasing pH.

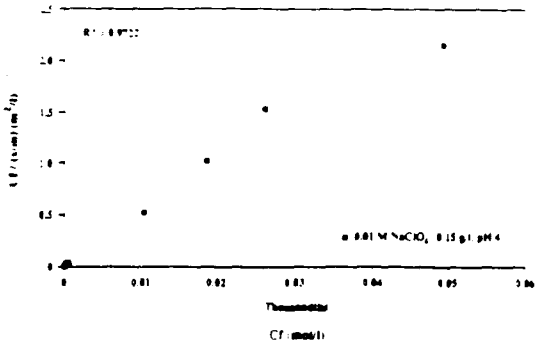

Figure 9. Langmuir isotherm data for arsenate adsorption on Fe_2O_3 particles (pH 4, 0.01 M $NaClO_4$, 4.5 mg/30 mL, 24-h equilibration).

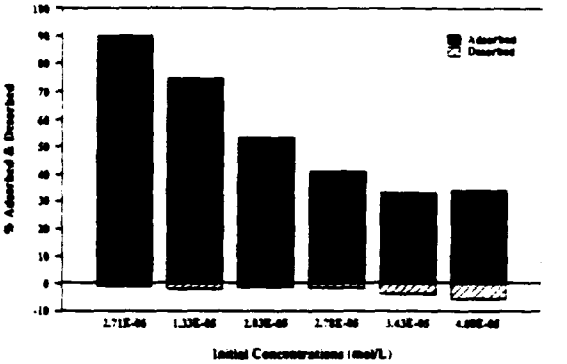

Figure 10. Adsorption–desorption data for arsenate on Fe_2O_3 particles (pH 7, 0.01 M $NaClO_4$, 4.5 mg/30 mL, 24-h equilibrations).

Desorption experiments using arsenate-free 0.01 M $NaClO_4$ at pH 7 indicated strong retention of the arsenate on the Fe_2O_3 particles, with only about 2–6% of the adsorbed fraction released. Percent desorption was directly proportional to the initial arsenate concentration, indicating a decline in the energy of adsorption as the surface became increasingly saturated with arsenate (Figure 10). This has important implications for pump-and-treat remediation of highly contaminated sites. High initial efficiency of dissolved arsenate removal will significantly decline once concentration values are reduced below the plateau portion of the adsorption isotherm and desorption becomes less energetically favorable.

Fe_2O_3–aquifer solid interaction experiments were performed in batch mode with different colloidal suspensions whose average size was 125 nm and particle concentration was 10 mg/L. A total of 53% of the particles heterocoagulated with the aquifer material in 0.01 M $NaClO_4$, whereas only 4% heterocoagulated in 0.01 M NaH_2PO_4. The percentage of initial particle concentration which interacted with the aquifer matrix solids was determined by difference between suspended particle activity and total initial activity. Blanks (no aquifer material) resulted in 3% loss.

Table II Column Results of Colloidal Fe_2O_3 Transport through Natural Aquifer Material

size, nm	pH	velocity, m day	particle concn, mg/L	ionic strength	anion	% C_0 thru	column length, cm
200	3.9	3.4	10	0.005	Cl^-	0	3.8
125	8.9	3.4	10	0.005	Cl^-	54	5.1
150	8.1	3.4	5	<0.001	ClO_4^-	57	3.8
250	8.1	3.4	10	0.03	SO_4^{2-}	17	3.8
150	8.9	3.4	5	0.03	SO_4^{2-}	14	3.8
100	7.6	3.4	5	0.03	$HAsO_4^{2-}$	97	2.5
100	7.6	1.7	5	0.03	$HAsO_4^{2-}$	96	2.5
100	7.6	0.8	5	0.03	$HAsO_4^{2-}$	93	2.5
125	7.6	3.4	10	0.03	HPO_4^{2-}	99+	5.1
100	7.6	1.7	5	0.03	HPO_4^{2-}	99	2.5
100	7.6	3.4	5	0.03	HPO_4^{2-}	99+	2.5

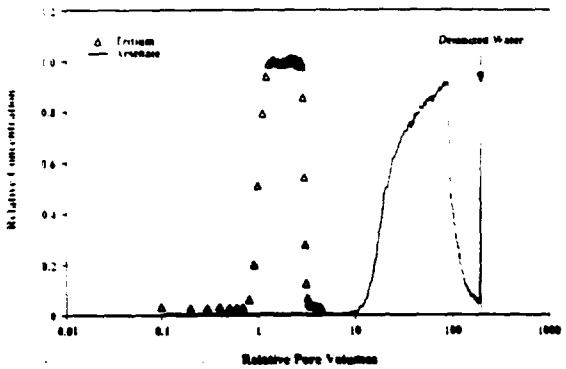

Figure 11. Breakthrough curve for dissolved arsenate versus tritiated water, and mobilization of colloidal-associated arsenate by deionized water.

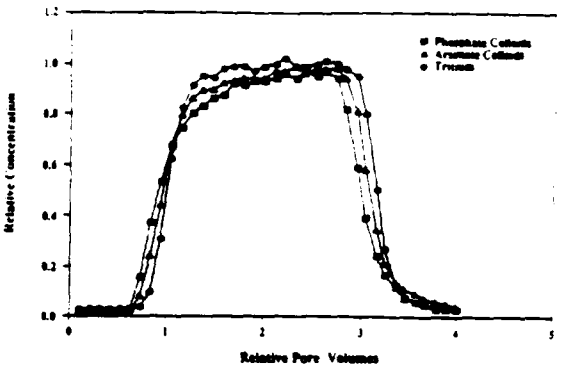

Figure 12. Breakthrough curve for Fe_2O_3 particles suspended in 0.01 M NaH_2PO_4 and in 0.01 M Na_2HAsO_4 (pH 7.8, 3.4 m/day, 5 mg/L).

Dissolved Arsenate Transport Experiments. Column studies with dissolved arsenate were performed to compare distribution factors (K_d) with those derived in the batch tests and for comparison to colloidal-facilitated transport of arsenate on the Fe_2O_3 particles. The column K_d roughly corresponds to the K value calculated using the Freundlich isotherm and is determined by

$$R_f = 1 + (\rho_b K_d / n) \quad (4)$$

where R_f is the retardation factor, ρ_b is the bulk density, and n is the porosity. Tritiated water was used for estimating the average bulk fluid velocity.

At a column flow rate of 3.4 m/day, ρ_b of 2.65 g/cm^3, and n of 0.4, the column K_d value was 1.4 L/kg. When the flow rate was decreased to 1.7 m/day, the column K_d value increased to 3.0 L/kg or approached those of the 24-h equilibrated batch K values. This indicated rate-limited adsorption onto the aquifer solids at the higher flow velocities. This demonstrates the importance of making such comparisons and not relying solely on batch sorption static equilibrium data, especially for specific site assessment purposes. When groundwater flow velocities are relatively rapid, assumptions of local equilibrium may be invalid. Flushing the columns with deionized water (low ionic strength) significantly increased turbidity in the column effluent due to dispersion of the aquifer fines. When the effluent was analyzed, the almost entirely colloid associated arsenate was determined to be approximately equal to the influent arsenate concentration, demonstrating the potential importance of this transport mechanism (Figure 11).

Colloidal Transport Experiments. The injected Fe_2O_3 particles generally broke through at the same time or prior to the tritiated water (Figure 12). The rate of colloid transport through the columns was over 21 times

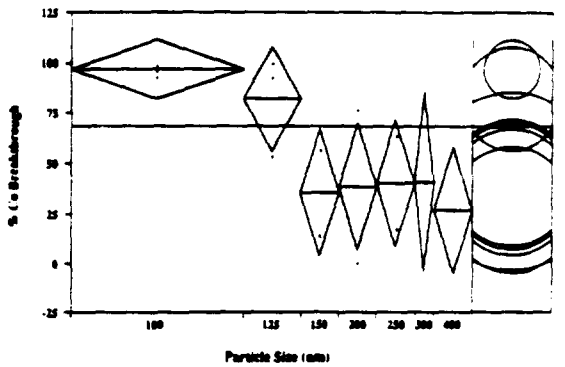

Figure 13. One-way ANOVA: effect of size on particle breakthrough (◇, 95% confidence interval; O, comparison of means).

faster than the dissolved arsenate. A summary of representative column results for the colloidal transport experiments is compiled in Table II. The extent of Fe_2O_3 particle breakthrough was dependent upon a variety of parameters. These parameters (Table II) were statistically explored in detail with the SAS program JMP, using % C_0 breakthrough as the response variable. Only particle size and anion significantly affected the % C_0 breakthrough (Figures 13 and 14) in these analyses. Within the different groupings (anion, size), the means and 95% confidence intervals are represented by horizontal lines within polygons. The concentric circles are simply overlays of the 95% confidence intervals. Combining these two parameters (anion and size) into a two-way main effects analysis of variance (two-way ANOVA) model accounts for 98.4% of the variability in the particle breakthrough results. The other factors tested gave no significant correlation over the parameter ranges utilized in this study. This is not to say

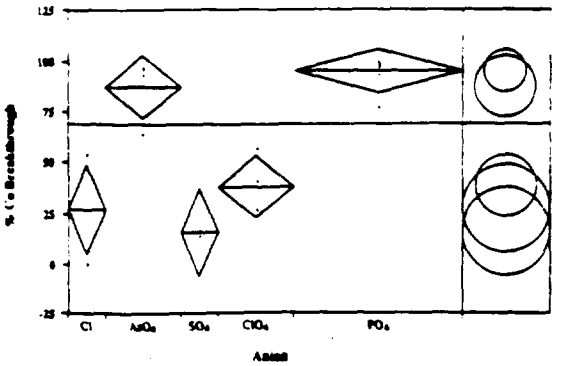

Figure 14. One-way ANOVA: effect of anion on particle breakthrough (◇, 95% confidence interval; O, comparison of means).

that the other factors were not important with respect to colloidal transport, only that anion and particle size most significantly affected particle breakthrough. Ionic strength and pH are obviously important factors affecting both colloidal stability and transport. In dilute solutions of nonspecifically bound electrolyte species a pH near the pH_{pzc} would preclude transport due to colloidal instability. Likewise, relatively high concentrations of phosphate and arsenate dramatically affect both colloidal stability (increase) and transport.

No colloidal transport occurred on the positive side of the iron oxide pH_{pzc}, indicating electrostatic interaction with the net negatively charged matrix material. In low ionic strength suspensions of NaCl and $NaClO_4$, transport exceeded 50% of initial particle concentrations. These results were in close agreement with the batch results (53%) on aquifer–colloid interactions. The increased negative surface charge on the particles in the phosphate suspensions resulted in increased repulsion between the Fe_2O_3 particles and the aquifer solids. This phenomenon permitted almost complete separation during settling in the batch tests and resulted in almost complete throughput in the column tests. There was substantially lower particle recovery of sulfate-based suspensions. The colloidal transport experiments with the sulfate-based suspensions, together with the results of colloidal stability experiments, suggest less specific interaction with the Fe_2O_3 surface compared to arsenate and phosphate.

Maximum percent breakthroughs occurred with phosphate- and arsenate-based suspensions and appeared to be unaffected by velocity (0.8–3.4 m/day) or column length. Likewise, no significant differences were observed due to particle concentration. Additional experiments are planned using longer columns to further explore particle flow path length and velocity effects on transport. The specific adsorption of the predominantly divalent phosphate and arsenate anions onto the Fe_2O_3 surface causes a charge reversal on the initially net positively charged surface and an increase in interparticle separation due to increased particle–particle repulsive forces. The effect is a lowering of the pH_{zpc} and an increase in net negative charge near the particle surface over a wider pH range. This also increased the repulsion between the mobile, negatively charged particles and the immobile, net negatively charged column matrix solids. As a result, the particles remain at a greater distance from the pore walls in the column matrix, where fluid velocity is higher. This charge exclusion, in addition to size-exclusion phenomena, may explain the early breakthrough of the colloids relative to the tritiated water. A comparison of colloidal breakthrough between phosphate and chloride suspensions is

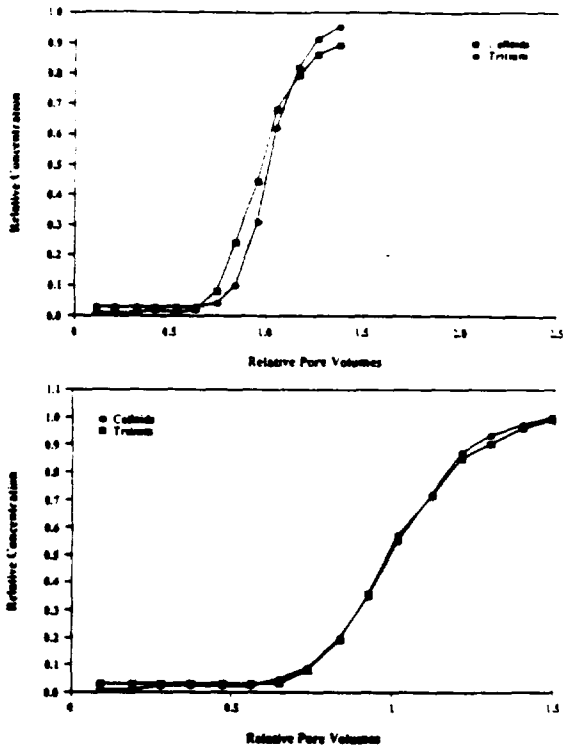

Figure 15. Comparison of Fe_2O_3 particle breakthrough in (a, top) 0.01 M NaH_2PO_4 and (b, bottom) 0.005 M NaCl suspensions.

shown in Figure 15. A greater exclusion volume is indicated where the only difference is the anionic composition of the supporting electrolyte.

Given a groundwater containing 20 mg/L suspended colloidal solids, of surface area and reactivity comparable to these Fe_2O_3 particles, approximately 0.1 mg/L arsenic could be colloidally transported under hydrogeochemical conditions represented by the 0.01 M $NaClO_4$ and 0.01 M NaCl suspension results described above. This is twice the current maximum contaminant level (MCL) currently set for drinking water. The reactivity of these model colloids compares favorably with some of the more ubiquitous subsurface minerals. Anderson et al. (*28*) determined aluminum hydroxide capacity for arsenate to be as high as 0.12 g/g. Hingston et al. (*29*) found the arsenate adsorption capacity for goethite to be on the order of 0.012 g/g. In addition, while this approximates the suspended solids concentration observed at the Arizona site it is only one-third the concentration observed at some other sites (*4*, *14*).

Summary and Conclusions

Transport of inorganic colloids through sand and gravel type aquifers may be significant under certain hydrogeochemical conditions. Due to the high reactivity of many inorganic particles in natural subsurface systems there is the potential that this form of contaminant transport may be important at select sites. Colloidal transport will be influenced by the following: ionic strength, ionic composition, flow velocity, quantity, nature, and size of suspended colloids, geologic composition and structure, and groundwater chemistry. The most significant of these factors under the conditions investigated in these column experiments were ionic composition and particle size. In some cases, neglecting colloidal mobility in our predictive contaminant transport models may underestimate both the

transport rate and mass flux. Chemical parameters affecting colloidal stability and transport must be included in transport modeling along with physical parameters (such as pore size distribution, colloidal density and size, and flow velocity).

Acknowledgments

We gratefully acknowledge the technical assistance efforts of Cynthia J. Paul of ManTech. and the ICP, AAGF, and radioanalytical support provided by Donald A. Clark of Robert S. Kerr Environmental Research Laboratory, U.S. EPA. We also acknowledge the support provided by Terry F. Rees, U.S. Geological Survey, San Diego, for SEM and XRD analysis. R.W.P. also thanks Jan Puls for her continued support, patience, and sacrifice.

Literature Cited

(1) Stumm, W.; Morgan, J. J. In *Aquatic Chemistry*, 2nd ed.; John Wiley and Sons, Inc.: New York, 1981; Chapter 10, p 647.
(2) Gschwend, P. M.; Reynolds, M. D. *J. Contam. Hydrol.* **1987**, *1*, 309–327.
(3) Robertson, W. D. *Ground Water* **1984**, *22*(2), 191–197.
(4) Ryan, J. N.; Gschwend, P. M. *Water Resour. Res.* **1990**, *26*, 307–322.
(5) Wellings, F. M. *Appl. Microbiol.* **1975**, *29*, 1751.
(6) Mack, W. N. *Health Serv. Rep.* **1972**, *87*, 271.
(7) Nightingale, H. I.; Bianchi, W. C. *Ground Water* **1977**, *15*(2), 146–152.
(8) Kim, J. I.; Buckau, G.; Baumgartner, F.; Moon, H. C.; Lux, D. Colloid Generation and the Actinide Migration in Gorleben Groundwaters. In *Scientific Basis for Nuclear Waste Management*; McVay, G. L., Ed.; Elsevier: New York, 1984; Vol. 7, pp 31–40.
(9) Torok, J.; Buckley, L. P.; Woods, B. L. *J. Contam. Hydrol.* **1990**, *6*, 185–203.
(10) Saltelli, A.; Avogadro, A.; Bidoglio, G. *Nucl. Technol.* **1984**, *67*, 245–254.
(11) Champ, D. R.; Merritt, W. F.; Young, J. L. Potential for Rapid Transport of Pu in Groundwater as Demonstrated by Core Column Studies. In *Scientific Basis for Radioactive Waste Management*; Elsevier: New York, 1982; Vol. 5, pp 745–754.
(12) Penrose, W. R.; Polzer, W. L.; Essington, E. H.; Nelson, D. M.; Orlandini, K. A. *Environ. Sci. Technol.* **1990**, *24*, 228–234.
(13) Enfield, C. G.; Bengtsson, G. *Ground Water* **1988**, *26*(1), 64–70.
(14) Buddemeier, R. W.; Hunt, J. R. *Appl. Geochem.* **1988**, *3*, 535–548.
(15) Puls, R. W.; Eychaner, J. H. Sampling of Ground Water for Inorganics—Pumping Rate, Filtration, and Oxidation Effects. In *Fourth National Outdoor Action Conference on Aquifer Restoration, Ground Water Monitoring and Geophysical Methods*; National Water Well Association: Dublin, OH, 1990.
(16) Yao, K.; Habibian, M. T.; O'Melia, C. R. *Environ. Sci. Technol.* **1971**, *5*, 1105–1112.
(17) O'Melia, C. R. *Environ. Sci. Technol.* **1980**, *14*, 1052–1060.
(18) Reynolds, M. D. *Colloids in Groundwater*. Masters Thesis, Massachusetts Institute of Technology, Cambridge, MA, 1985.
(19) Nuttall, H. E. *Interim Report on Particulate Transport*. Milestone No. T424, TWS-ESS-5/9-88-06, Los Alamos National Laboratory, Los Alamos, NM, December 1988.
(20) Cerda, C. M. *Colloids Surf.* **1987**, *27*, 219–241.
(21) Eichholz, G. G.; Wahlig, B. G.; Powell, G. F.; Craft, T. F. *Nucl. Technol.* **1982**, *58*, 511–519.
(22) Champlin, J. B. F.; Eichholz, G. G. *Health Phys.* **1976**, *30*, 215–219.
(23) Matijevic, E.; Kuo, R. J.; Kolny, H. *J. Colloid Interface Sci.* **1988**, *80*, 94–106.
(24) Puls, R. W.; Eychaner, J. H.; Powell, R. M. *Colloidal-Facilitated Transport of Inorganic Contaminants in Ground Water: Part I. Sampling Considerations*; EPA/600/M-90/023; USEPA Environmental Research Brief, 1990.
(25) Neaville, C. C. U.S. Geological Survey, written communication, 1990.
(26) Matijevic, E.; Scheiner, P. *J. Colloid Interface Sci.* **1978**, *63*, 509–524.
(27) Liang, L.; Morgan, J. J. *Aquat. Sci.* **1990**, *52*, 32–55.
(28) Anderson, M. A.; Ferguson, J. F.; Gavis, J. *J. Colloid Interface Sci.* **1976**, *54*, 391–399.
(29) Hingston, F. J.; Posner, A. M.; Quirk, J. P. *Discuss. Faraday Soc.* **1971**, *52*, 334–342.

Received for review April 4, 1991. Revised manuscript received September 24, 1991. Accepted November 6, 1991. Although the research described in this article has been funded wholly or in part by the United States Environmental Protection Agency, it has not been subjected to the Agency's peer and administrative review and therefore may not necessarily reflect the views of the Agency and no official endorsement may be inferred.

